



Hourly Day Ahead Solar Irradiance Forecasting Model in LabVIEW Using Cloud Cover Data

Oguzhan CEYLAN¹, Michael STARKE², Phil IRMINGER², Ben OLLIS², Dan KING² and Kevin TOMSOVIC³

¹Istanbul Kemerburgaz University, Istanbul, Turkey

²Oak Ridge National Laboratory, Oak Ridge, USA

³The University of Tennessee, Knoxville, USA

oguzhan.ceylan@kemerburgaz.edu.tr, starkemr@ornl.gov, irmingerp@ornl.gov, ollistb@ornl.gov, kingdj@ornl.gov, tomsovic@utk.edu

Abstract: This paper applies a regression based numerical method for hourly forecasting photovoltaic power output. This methodology uses a historical dataset composed of irradiance, azimuth, zenith angle and time of day information. A developed forecast program from this methodology pulls publicly available cloud cover forecast data for the following day and uses a numerical regression based method for fitting the data. Using publicly available temperature forecast data, forecasted irradiance data, and computed solar position (zenith, azimuth) data, both power output and temperature module output of PV array is computed. Numerical forecast results are compared to actual collected data.

Keywords: solar forecasting, numerical regression, LabVIEW.

1. Introduction

With the power grid evolving to more renewable based resources, the usage of photovoltaic (PV) technologies is steadily increasing. The world's energy needs are projected to be 30 TW in 2050 (triple the usage of 2011) and with a focus to reduce CO₂ emissions PV installations are expected to expand [1]. Solar technology efficiency increases and lowered cost have made significant progress towards wider industry acceptance. However PV is unlike conventional power plants, power output of PV generation systems is not externally controlled or constant in time. Changes in cloud cover create intermittent irradiance on the PV panels, which lead to power fluctuations from the PV systems. The impact of solar penetration into power systems is detailed in [2].

Spinning and non-spinning reserves in electrical power systems may overcome this output challenge. For example, energy storage is becoming popular as a spinning reserve solution. These assets incur additional costs to the overall system. As a first measure to overcome the power output challenges, accurate PV forecasting is vital.

PV output needs accurate forecasting for efficient operation of electric power systems. Several methods have been used in PV power forecasting. One of these methods is time series modeling [3] and in [4] different time series models are compared. In [5] the power

output of a PV system is forecasted by using artificial neural networks referencing only the historical data of the PV system. The work in [6] uses solar irradiance and temperature data together with artificial neural networks. In [7] hourly forecast prediction using artificial neural networks and wavelet transform is discussed. Genetic algorithms are shown to provide the best simulation results in [8] when used with artificial neural networks. In [9] Kalman Filters are used for forecasting. Another tool used to forecast PV power output is support vector machines [10, 11]. Detailed information on solar irradiance forecasting methods may be found in [12, 13].

According to [12] global horizontal irradiance (GHI) forecasting approaches may be applied from very short timescales from 5 minutes to 6 hours where artificial neural networks and autoregressive and autoregressive moving average models are used. For irradiance forecasting information of cloud cover is needed. This cloud cover data may be found either in satellite images or ground-based sky images. The study [14] uses cloud motion vectors from satellite images and shows good performance for periods from 30 minutes to 6 hours ahead. Ground-based sky images may be used for very short term irradiance forecasting [15].

This study presents an extended computational approach to forecast PV output by using a numerical regression method [16]. Since the solar irradiance of an area is based on the positions and angles (longitude, latitude, azimuth, zenith), these components are involved in the forecasting

processes. This method uses publicly available, daily, hour-based cloud cover forecast data and temperature forecast data. Different from previous work [17], where neural networks are used in the forecasting phase, a numerical regression algorithm is applied. After obtaining the next day's forecasted irradiance values, the model uses a Newton-Raphson model-based maximum power point tracking (MPPT) algorithm for PV power output calculation. The PV module temperature model uses publicly available temperature forecasts together with the calculated power output forecasts. LabVIEW is used as the programming environment.

The following sections describe the model for PV power output and module temperature forecast. The subsections describe the data and the preparation and calculation processes. The final section compares the test results to the actual data collected.

2. The Model

A model is developed in LabVIEW for PV panel power output and module temperature output forecast. The flowchart of the model is shown in Figure (1). The first step is to collect cloud cover data from the Web. A function is used to calculate the azimuth and zenith angles of each hour in the next day using the longitude and latitude information of the current location. With these data points, and the historical data composed of azimuth, zenith, hour of day, and cloud cover data, irradiance values are forecasted by using a numerical

regression algorithm. The final step includes the calculation of MPPT and module temperature by using the calculated irradiance forecasts and temperature forecasts obtained from the Web. The LabVIEW snapshot of the main program is given in Figure (2). The following subsections describe these steps.

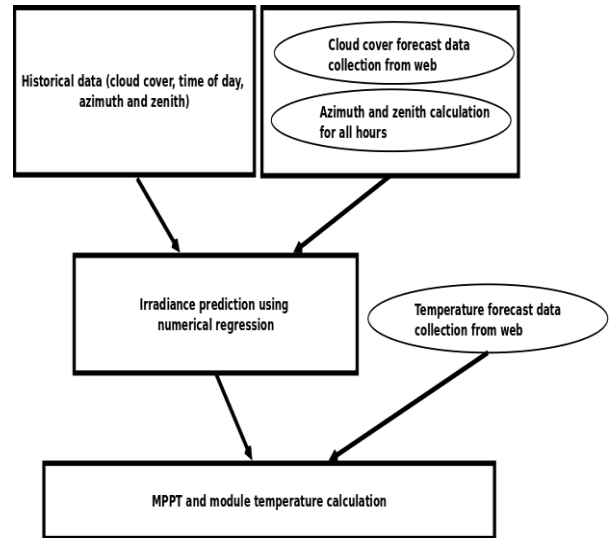


Figure 1. Flowchart of PV power output and module temperature forecast model.

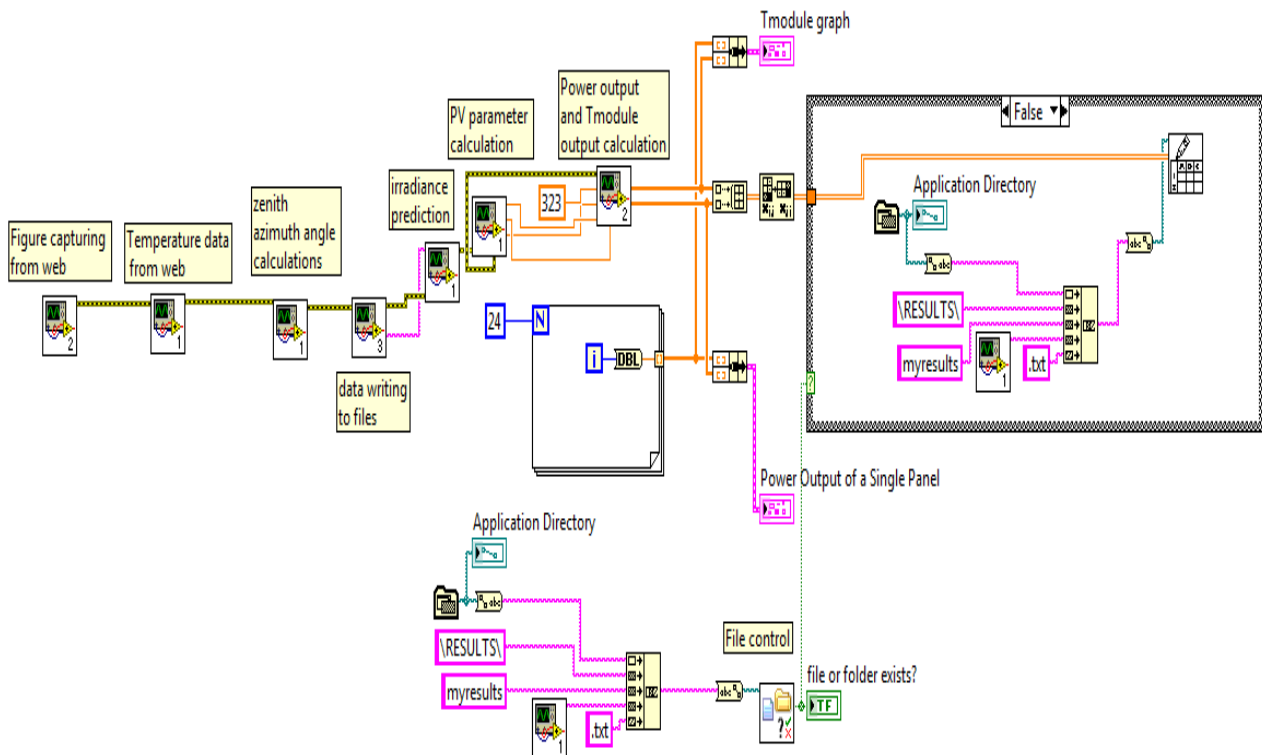


Figure 2. LabVIEW PV power output and module temperature forecast program

2.1. Cloud Cover Data Collection

The cloud cover forecast data is obtained from publicly available data from the Web [18]. Figure (3) shows a forecasted satellite image of the U.S. Southeast. The longitude and latitude coordinates for Oak Ridge where the Distributed Energy Communications and Control (DECC) Lab is located is represented with a black star on the image. On the right hand side of the image the legend shows the colors and cloud cover percentage equivalents. The process for finding the cloud cover forecast data for the next day is as follows:

- Connect to the cloud cover forecast webpage.
- The available images that have cloud cover forecast data start from 3 am of the current day and continue until the end of next day. Download the cloud cover forecast images to the computer that runs the forecasting program.
- Store values of cloud cover percentage by using the coordinate information of ORNL's DECC Lab, the corresponding pixel values, and the legend colors which specify the cloud cover percentages for each image.

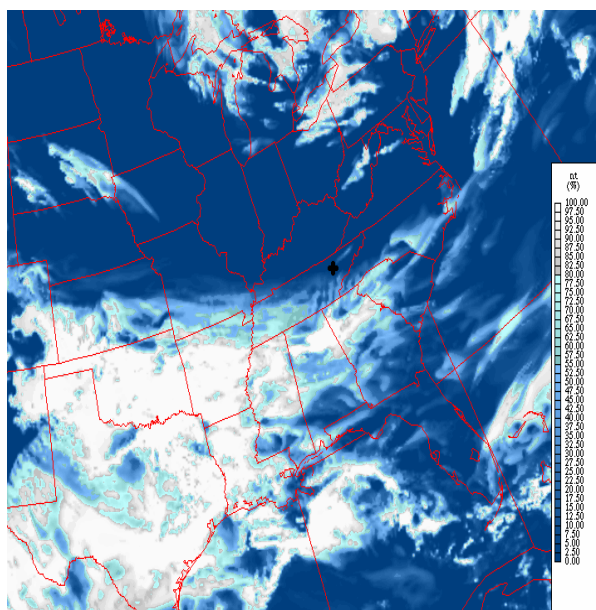


Figure 3. A sample cloud cover image of U.S. Southeast and the position of ORNL's DECC Lab.

2.2. Azimuth and zenith angle calculation

A MATLAB function based on [19] written by Vincent Roy was translated into LabVIEW. The function uses year, month, day, hour, minute, second, time difference from Greenwich, latitude, longitude, and altitude of the location as inputs. The outputs of the function are zenith and azimuth angles in degrees. For each day to be forecasted, the function is run with one hour intervals.

2.3. Irradiance Forecast Using Numerical Regression

Forecasting the solar irradiance includes two steps. The first step is to pull the saved data collected from the actual PV system as historical data. The second step forecasts the irradiance values using the historical data and a numerical regression-based model. The historical information is fit into the forecasted function values.

2.3.1. Historical Data

A dataset consisting of actual values of time of day, cloud cover forecasts, and azimuth and zenith angles for 40 days was used. A sample plot of historical irradiance values measured is shown in Figure (4).

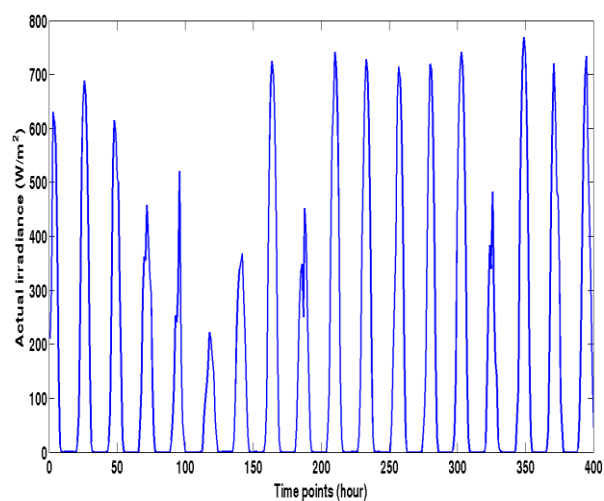


Figure 4. Sample actual historical data (irradiance values).

2.3.1. Irradiance Forecasting

It is known that in a multiple regression model, a measurement Y is related to several predictors X_i for each observation. It is obvious that irradiance forecasting regression process will be dependent to more than one variable. This study uses time of the day, cloud cover percentage, azimuth and zenith angles in the forecasting process. A general function to be used in the forecasting process is shown as follows:

$$Y = \alpha_1 + \sum_{j=2}^n \alpha_j f(x_j) + Error \quad (1)$$

By using equation (1), a model needs to be proposed. The approach for obtaining a proper model for forecasting is to find a function that fits as close as possible to the past data. For this aim, several different combinations of functions composed of time of day, cloud cover, azimuth and zenith angle were used. To catch the nonlinear behaviors such as sharp fluctuations of the irradiance, several different linear and nonlinear combinations of the components were included in the forecasting model. The final model to be used for fitting the data is given below:

$$\begin{aligned}
 F = & \alpha_1 + \alpha_2 \times e^{\frac{t}{50}} \times \sin(t) + \alpha_3 \times c + \alpha_4 \times z \\
 & + \alpha_5 \times a + \alpha_6 \times t^2 + \alpha_7 \times z^2 + \alpha_8 \times t + \alpha_9 \times \\
 & \cos(c) + \alpha_{10} \times z \times \sin(t) + \alpha_{11} \times a \times \sin(t)^2 \\
 & + \alpha_{12} \times e^{\frac{z}{1000}} \times \sin(t) + \alpha_{13} \times e^{\frac{a}{100}} \times \sin(t) \\
 & + \alpha_{14} \times e^{\frac{z}{100}} \times \sin(c) + \alpha_{15} \times e^{\frac{a}{100}} \times \sin(c) \\
 & + \alpha_{16} \times c \times \sin(t) + \alpha_{17} \times z \times t + \alpha_{18} \times z \times c \\
 & + \alpha_{19} \times e^{\frac{z}{100}} \times \cos(t) + \alpha_{20} \times e^{\frac{a}{100}} \times \cos(t) \\
 & + \alpha_{21} \times e^{\frac{z}{100}} \times \cos(c) + \alpha_{22} \times e^{\frac{a}{100}} \times \cos(c) \\
 & + \alpha_{23} \times \sin(z) + \alpha_{24} \times \sin(a) + \alpha_{25} \times e^{\frac{z}{100}} \\
 & \times \tan(t) + \alpha_{26} \times \cos(z)^2 + \alpha_{27} \times \cos(a)^2 \\
 & + \alpha_{28} \times e^{\frac{a}{100}} \times \cos(c)^2 + \alpha_{29} \times e^{\frac{a}{100}} \times \cos(t)^2 \quad (2)
 \end{aligned}$$

Where t , c , a , and z represent time, cloud cover, azimuth, and zenith respectively. The algorithm for forecasting the next day's irradiance values is as follows:

- For all data points of 40 days, calculate the value of the following function and store in a vector V .

$$\begin{aligned}
 F = & 1 + e^{\frac{t}{50}} \times \sin(t) + c + z + a + t^2 + z^2 \\
 & + t + \cos(c) + \sin(t) + a \times \sin(t)^2 + e^{\frac{z}{1000}} \\
 & \times \sin(t) + e^{\frac{a}{100}} \times \sin(t) + e^{\frac{z}{100}} \times \sin(c) + \\
 & e^{\frac{a}{100}} \times \sin(c) + c \times \sin(t) + z \times t + z \times \\
 & c + e^{\frac{z}{100}} \times \cos(t) + e^{\frac{a}{100}} \times \cos(t) + e^{\frac{z}{100}} \\
 & \times \cos(c) + e^{\frac{a}{100}} \times \cos(c) + \sin(z) + \\
 & \sin(a) + e^{\frac{z}{100}} \times \tan(t) + \cos(z)^2 + \\
 & \cos(a)^2 + e^{\frac{a}{100}} \times \cos(c)^2 + e^{\frac{a}{100}} \times \cos(t)^2
 \end{aligned} \quad (3)$$

- Calculate the α coefficient as follows:
 $\alpha = (V' \times V)^{-1} \times V' \times G$ (4)
 where G is a vector of elements consisting of the actual irradiance values for 40 days of data.
- Using the computed α values and the function given above predict the next day's irradiance values using equation (2).

2.4. Temperature Forecasts

Temperature forecasts are performed by getting data from [20]. The process starts by computing the number of days from the beginning of the current year, and that day's forecast data. The target webpage is reached using LabVIEW and the code of the page is assigned to a string variable. Specific hour temperature values are sought in this string systematically and interpolation is used to obtain the next day's temperature forecasts. A sample temperature forecast webpage that is used in obtaining this data is shown in Figure (5).

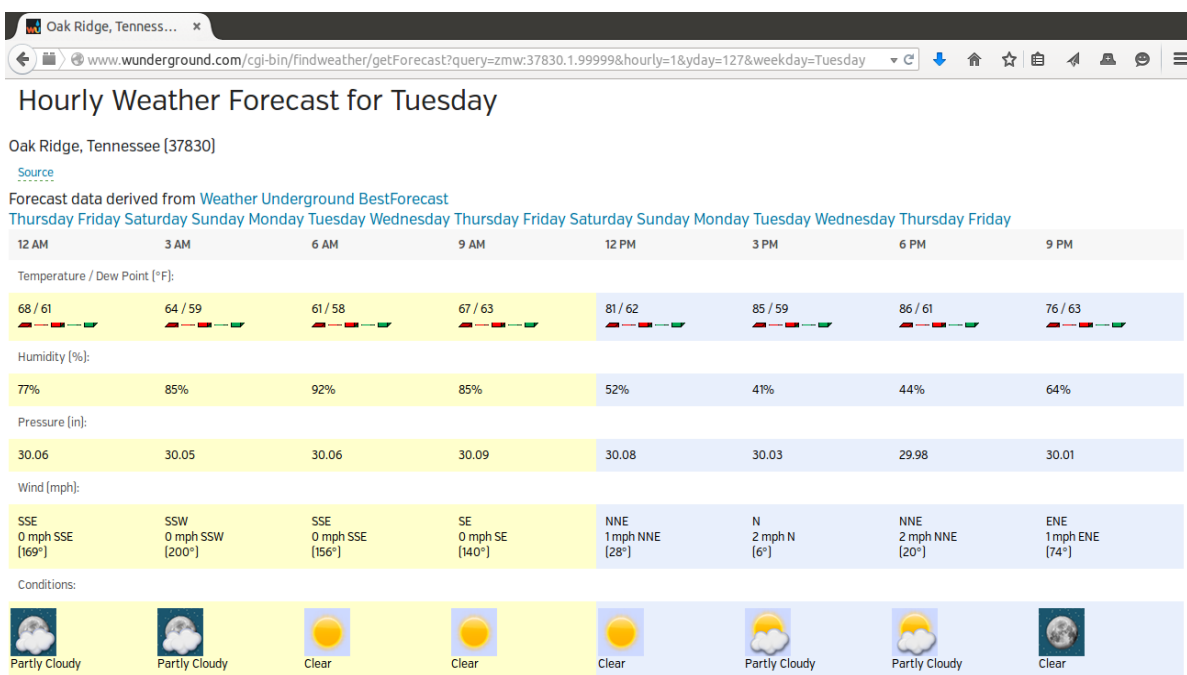


Figure 5. A sample temperature forecast webpage.

2.4. MPPT and MPPT Temperature Module Calculation

The model in [21] was used for the calculation of the MPPT. This model uses a PV circuit model comprising of a diode and series and parallel resistances as shown in Figure (5).

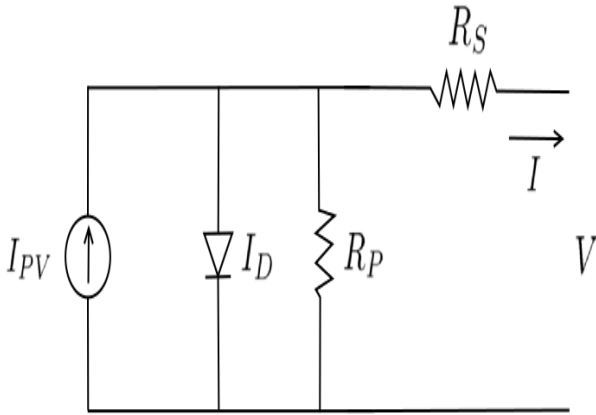


Figure 5. Single diode PV representation.

The output current of the PV module is computed by using Kirchoff's Current Law. Numerically, this process requires subtracting the sum of diode current and the current passing through parallel resistance from the photovoltaic current as represented in equation (5):

$$I = I_{pv} - I_0 \left[e^{\frac{V + R_s I}{V_t \alpha}} - 1 \right] - \frac{V + R_s I}{R_p} \quad (5)$$

Where I_{pv} and I_0 are the photovoltaic and saturation currents of the PV array respectively. $V_t = N_s k T$ is the thermal voltage (with N_s cells in series connection), R_s and R_p are equivalent series and parallel resistances, and α is the diode constant whose typical value lies between 1 and 1.5

2.5.1. Determining $R_s, R_p, P_{max}, I_{pvmax}$

Several parameters such as: K_v open circuit voltage temperature coefficient, K_I short-circuit current temperature coefficient, $V_{oc,n}$ nominal open circuit voltage, $I_{sc,n}$ nominal short-circuit current, V_{mp} voltage at the maximum point, I_{mp} current at maximum point are known. Other constants are k Boltzmann's Constant and q electron charge. Parameters for the model can be found on the 280 W Hanwa Solar PV data sheet and are provided in Table (1) as reference [17]:

Table 1. HSL72 Solar PV Module Parameters

Definition	Value
Maximum Power (P_{max})	280 W
Voltage at maximum power (V_{mp})	35.7 V
Current at maximum power (I_{mp})	7.84 A
Voltage at Open Circuit (V_{oc})	44.6 V
Current at Open Circuit (I_{sc})	8.43 A
K_I	0.005058 A/K
K_v	-0.14718 V/K
N_s	72

In the computations, the diode saturation current given below is also used:

$$I_0 = \frac{I_{sc,n} + K_I \Delta T}{e^{\frac{V_{oc,n} + K_v \Delta T}{\alpha V_t}} - 1} \quad (6)$$

where $\Delta T = T - T_n$ represents the difference between the ambient and the nominal temperature. Hence, the temperature has an effect on diode saturation current.

The process for determining the series and parallel resistances, maximum power and maximum photovoltaic current starts with initially setting R_s to 0, and R_p to $\frac{V_{mp}}{I_{sc,n} - I_{mp}} - \frac{V_{oc,n} - V_{mp}}{I_{mp}}$. Then by selecting a small step size of R_s , such as 0.003, R_s is slowly increased and in each step the following operations are performed.

$$I_{pv,n} = \frac{R_p + R_s}{R_p} I_{sc,n} \quad (7)$$

$$I_{pv} = (I_{pv,n} + K_I \Delta T) \frac{G}{G_n} \quad (8)$$

where G is the actual irradiance and G_n is the nominal irradiance.

$$R_p = \frac{V_{mp}(V^-)}{V_{mp} I_{pv} - V_{mp} I_0 e^{\frac{V^- - q}{\alpha N_s K T}} + V_{mp} I_0 - P_{max}} \quad (9)$$

where $V^- = (V_{mp} + I_{mp} R_s)$.

- Equation (4) is solved for all V values from 0 to $V_{oc} N_{ser}$ by using Newton-Raphson method and for each V value, a I value is obtained, computing all the power values for these pairs. The maximum power value is computed and stored.

From all the maximum powers, there is only one point that satisfies the condition $P_{max,m} = V_{mp} I_{mp}$

$P_{max,m} = V_{mp} I_{mp}$ at the (V_{mp}, I_{mp}) point [18]. Using $P_{max}=6719.82$, position =102, $R_s=0.306$, $R_p=573.91$, and $I_{pvmax}=8.47345$ are found. The graph of P_{max} as a function of R_s is shown in Figure (7).

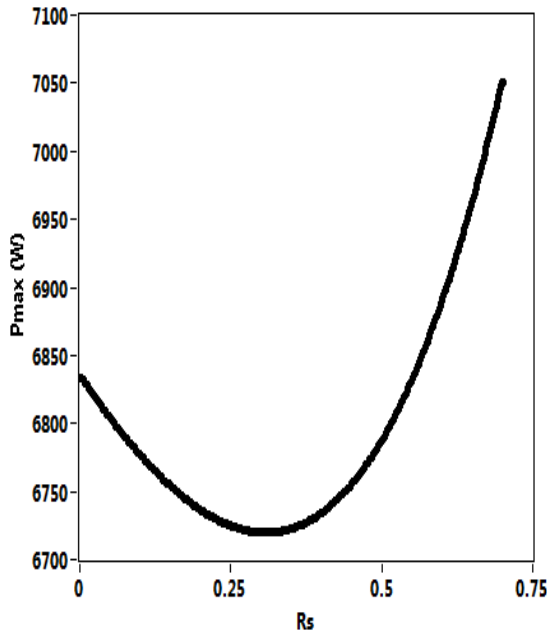


Figure 7. P_{max}, R_s graph.

2.5.2. Calculation of PV Power Output

PV power output calculations use R_p, R_s, I_{pvmax} , ambient temperature T , and irradiance G as inputs. P and T_{module} are the outputs.

A thermal calculation model for a PV module is given in [21]. This model takes the decrease and increase in the temperatures into consideration for module temperatures. The change in module temperature is given by the following equation:

$$C_{module} = q_{lw} + q_{sw} + q_{conv} - P_{out} \quad (10)$$

where $C_{module}, q_{lw}, q_{sw}, q_{conv}$ and P_{out} represent the heat capacity of the module, short wave transfer, convection heat transfer, and power generated by the module respectively. Detailed information on these equations may be found in [22].

The algorithm for calculation of PV power output and module temperature is given in Algorithm 1. As seen below, the algorithm includes a main for loop for 24 hour simulation and two sub for loops. The first sub loop performs PV power output calculation by using Newton-Raphson method, and the second sub loop calculates module temperature by using Euler's Method. The first sub loop uses R_p, R_s, I_{pvmax}, T , and G as input values. The second sub loop uses the power output from the first sub loop. Other inputs are the ambient temperature and forecasted irradiance value. Note that the simulations are performed for each hour of the day and module temperatures are calculated for the end of each simulation hour.

```

Inputs:  $R_p, R_s, I_{pvmax}, T, G$ 
Outputs:  $I, V, P, T_{module}$ 
for Day of Time=1:23 do
  for  $V = 0 : V_{oc,n}Ns$  do
    Inputs:  $R_p, R_s, I_{pvmax}, T, G$ 
    Outputs:  $I, V, P$ 
    Solve equation 5 with Newton Raphson Method using
    numerical derivatives: That is  $I_{i+1} = I_i - \frac{f(I)}{f'(I)}$  and
     $f'(I) = \frac{f(I+h)-f(I)}{h}$  where  $h$  is a small number.
    From each  $V, I$  pairs find  $P_{max}$ 
  end
  for Time = 0 : 3600s do
    Inputs:  $G, T_{ambient}, P$ 
    Outputs:  $T_{module}$ 
    Solve equation 10 by using Euler Method. That is
     $T_{module(i+1)} = T_{module(i)} + \text{step}f'(T_{module(i)})$  and
     $f'(T_{module}) = \frac{f(T_{module}+h)-f(T_{module})}{h}$  where, step is a user defined
    step number and  $h$  is a small number.
  end
end

```

Algorithm 1. PV output and temperature module calculation algorithm.

A sample $V-I$ graph for different irradiance values is shown in Figure (8). Simulations are performed for irradiance values changing from 200 to 1000 W/m^2 for this specific example. As expected the current increases as the irradiance input increases.

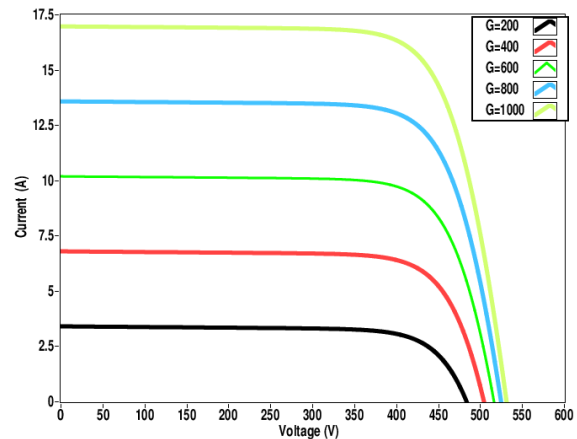


Figure 8. V, I graph for different G values

Figure (9) shows the effect of irradiance values ranging from 0 to 1000 W/m^2 and current outputs ranging from 0 to 17.5A on module temperature. In this simulation ambient temperature is kept constant. In this case higher irradiance values result in higher module temperature values.

Figure (10) shows the effects of irradiance values ranging from 307.5 to 310 K on module temperature. Power output is kept constant in this simulation. As shown, as the ambient temperature increases, the module temperature increases. Similarly, higher irradiance values produce higher module temperatures.

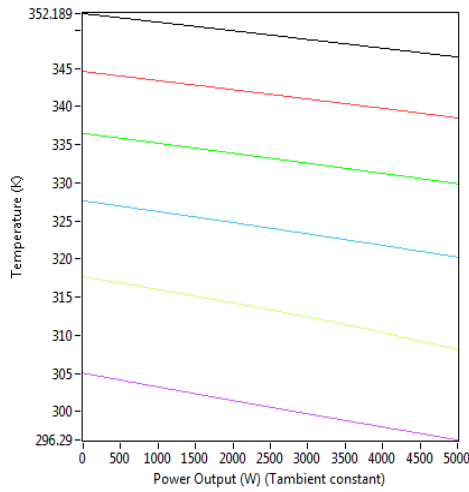


Figure 9. The effect of irradiance and power output on module temperature.

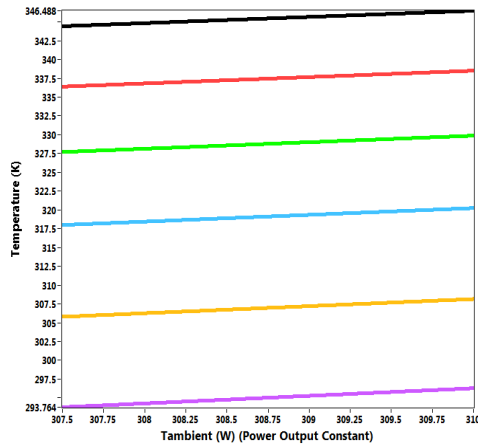


Figure 10. The effect of irradiance and ambient temperature on module temperature.

3.1. Tests and Results

The proposed method was tested from 24th to 30th of June 2015. RMSE (root mean square error) and nRMSE (normalized root mean square error) results are calculated.

Simulation results are compared to actual values obtained from the PV module installed on ORNL’s DECC Lab. In Figure (11), the actual and forecasted irradiance values for the specified days are shown. Comparison of the measurements to the forecast shows that clear days lead to more accurate forecasts than cloudy days. From the figure, the highest irradiance error is obtained for 29th of June. The reason for the discrepancy is either cloud cover forecast errors or irradiance measurement errors. The RMSE and nRMSE values for 7 days irradiance simulation is calculated as 141.83 W/m² and 0.45 respectively.

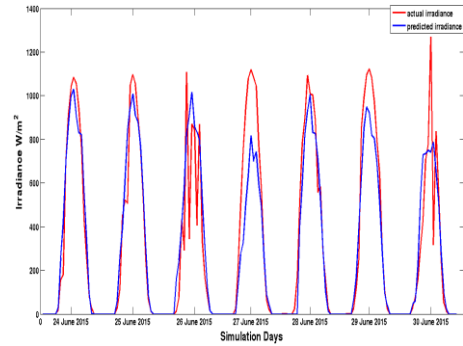


Figure 11. Actual and forecasted irradiance values for 24th to 30th of June 2015.

Figure (12) illustrates actual and forecasted power output of a single PV panel. The power output forecasts of the PV panel match with the actual results. The error increases for the days that have more fluctuations in power output. Since the model uses forecasted cloud cover in forecasting solar irradiance, this also increases the error. The RMSE and nRMSE values for power output are found as 1252.41W and 0.9984 respectively.

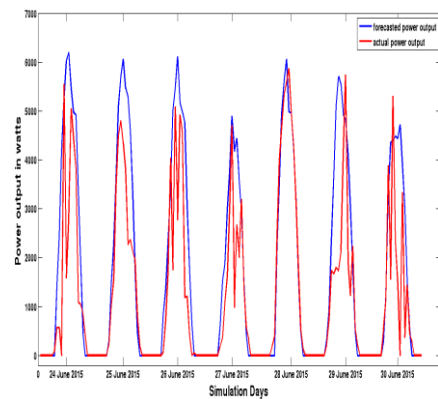


Figure 12. Actual and forecasted power values for 24th to 30th of June 2015.

Figure (13) shows the actual and the forecasted temperatures of the PV module. The forecasted temperature module temperatures represent the behavior of the actual module temperatures. The RMSE and nRMSE one week values for module temperature is computed as 7.96C and 0.2514 respectively.

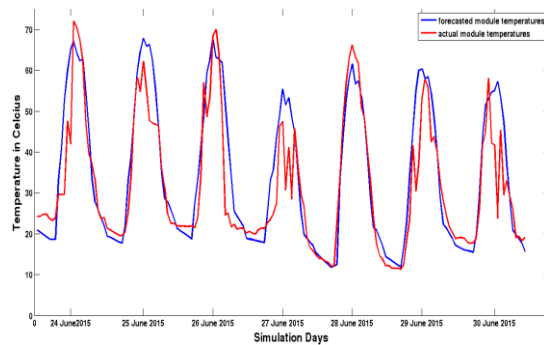


Figure 13. Actual and forecasted module temperatures for 24th to 30th of June 2015.

4. Conclusion

This paper uses a numerical regression method for PV output and module temperature output forecasting. The computation model uses publicly available cloud cover forecast information and temperature forecast data together with position and angle components such as longitude, latitude, azimuth, and zenith to perform the forecasts. LabVIEW is used as simulation tool and to our knowledge there is no other work that uses LabVIEW as the simulation tool.

A sample of one week's simulation results show that the irradiance and module temperature forecasting match well with actual results. These forecast results are planned to be used in a microgrid operation and control environment. Since the simulations are performed aiming at the next day's forecast, these results will help in optimizing resource dispatch in the microgrid.

5. References

- [1] T. M. Razykov, C. S. Ferekides, D. Morel, E. Stefanakos, H. S. Ullal and H. M. Upadhyaya, "Solar photovoltaic electricity: current status and future prospects", *Solar Energy*, vol. 85: 8, pp. 1580-1608, August 2011.
- [2] D. Lew, N. Miller, K. Clark, G. Jordan, Z. Gao, "Impact of high solar penetrations in the western interconnection.", Technical Report, National Renewable Energy Laboratories NREL/TP-5500-49667, 2010
- [3] P. Bacher, H. Madsen, and H. A. Nielse, "Online short-term solar power forecasting", *Solar Energy*, vol. 83:10 pp. 1772–1783, 2009
- [4] G. Reikard, "Predicting solar radiation at high resolutions: a comparison of time series forecasts", *Solar Energy*, vol. 83:3 pp. 342–349, 2009
- [5] M. Ding, L. Wang, and R. Bi, "An ANN based approach for forecasting the power output of photovoltaic system", *Procedia Environmental Sciences*, vol. 11 pp. 1308–1315, 2011
- [6] A. Mellit, and A. M. Pavan, "A 24-h forecast of solar irradiance using artificial neural network: Application for performance prediction of a grid connected PV plant at Trieste, Italy", *Solar Energy*, vol. 84 pp. 807–821, 2010
- [7] P. Mandal, S. T. S. Madhira, A. U. I. Haque, J. Meng, R. L. Pineda, "Forecasting power output of solar photovoltaic system using wavelet transform and artificial intelligence techniques", *Procedia Comput. Sci.* vol.12, 332337 2012.
- [8] H. T. C. Pedro, C. F. M. Coimbra, "Assessment of forecasting techniques for solar power production with no exogenous inputs", *Solar Energy* vol.86, pp.2017-2028 2012
- [9] S. Pelland, G. Galanis, and G. Kallos, "Solar and photovoltaic forecasting through post-processing of the Global Environmental Multiscale numerical weather prediction model". *Progress in Photovoltaics: Research and Applications* vol. 21:3 pp. [284–296 2011](#)
- [10] J. Shi, W. Lee, Y. Lee, Y. Yang and P. Wang, "Forecasting power output of photovoltaic systems based on weather classification and support vector machines". *IEEE Transactions on Industry Applications* vol. 48:3 pp. 1064–1069 2012
- [11] J. G. Da Silva Fonseca, T. Oozeki, T. Takashima, G. Koshimizu, Y. Uchida, and K. Ogimoto, "Use of support vector regression and numerically predicted cloudiness to forecast power output of a photovoltaic power plant in Kitakyushu, Japan" *Prog. Photovolt. Res. Appl.* 2012, 20, pp. 874-882.
- [12] M. Diagne, M. David, P. Lauret, J. Boland and N. Schmutz, "Review of solar irradiance forecasting methods and a proposition for small-scale insular grids", *Renewable and Sustainable Energy Reviews*, vol. 27, pp 65–76, November, 2013.
- [13] B. Espinar, J. L. Aznarte, R. Girard, A. M. Moussa, G. Kariniotakis. "Photovoltaic Forecasting: A state of the art", 5th European PV-Hybrid and Mini-Grid Conference OTTI – Ostbayerisches Technologie-Transfer-Institut, Tarragona, Spain. pp.250–255, 2010
- [14] E. Lorenz, A. Hammer, D. Heinemann D., "Short term forecasting of solar radiation based on satellite data". *EUROSUN 2004 (ISES Europe Solar Congress)* 2004:8418.
- [15] C. W. Chow, B. Urquhart, M. Lave, A. Domingues, J. Kleissi, J. Shields, and B. Washom "Intra-hour forecasting with a total sky imager at the UC San Diego solar energy testbed", *Solar Energy* vol. 85:11, pp. 2881–2893 2011
- [16] O.Ceylan, M. Starke, P. Irrminger, B. Ollis, K. Tomsovic, "A Regression Based Hourly Day Ahead Solar Irradiance Forecasting Model by Labview Using Cloud Cover Data", *International Conference on Electrical and Electronics Engineering*, Eleco November 2015.
- [17] M. Starke, J. Nutaro, T. Kuruganti and D. Fugate, "Integration of photovoltaics into building energy usage through advanced control of rooftop unit", *International High Performance Buildings Conference*, Purdue, 2014
- [18] <http://weather.gc.ca>
- [19] I. Reda, A. Andreas, A. "Solar position algorithm for solar application." NREL, Technical Report, 2003
- [20] <http://wunderground.com>
- [21] M. G. Villalva, J. R. Gazoli, E. R. Filho, "Modeling and circuit-based simulation of photovoltaic arrays", *COBEP 09 Power Electronics Conference*, vol. 27, pp 1244–1254, Sep 27 2009- Oct 1 2009.
- [22] A.D. Jones, C.P. Underwood, A therma l model for photovoltaic systems, *Solar Energy*, Vol.70:4 pp. 349–359 2001.

5. Acknowledgements

This work was sponsored by the Office of Electricity Delivery & Energy Reliability, U.S. Department of Energy under Contract No. DE-AC05-00OR 22725 with UT-Battelle and conducted at ORNL and UT Knoxville. This work also made use of Engineering Research Center Shared Facilities supported by the Engineering Research Center Program of the National Science Foundation and the Department of Energy under NSF Award Number EEC-1041877 and the CURENT Industry Partnership Program. The first author would like to thank the Scientific and Technological Research Council of Turkey (TUBITAK) for its financial support.